Journal of Hydroscience and Hydraulic Engineering
Vol.21, No.1 May, 2003, 63-70

EXPERIMENTAL STUDY OF INTERFACIAL TURBULENT STRUCTURES IN WIND-INDUCED WATER WAVES BY SYNCHRONOUS LDA MEASUREMENTS

By

Iehisa NEZU

Professor, Dept. of Civil & Global Environmental Eng., Kyoto University, Kyoto 606-8501, Japan

Keisuke YOSHIDA and Daisuke IKEDA

Graduate Student, Dept. of Civil & Global Environmental Eng., Kyoto University, Kyoto 606-8501, Japan
E-mail: nezu@nezu.gee.kyoto-u.ac.jp, Fax: (+81) 75-753-5066

SYNOPSIS

This paper describes an experimental study on mutual turbulent interactions across the air-water interface in the wind-induced water waves by using two sets of synchronous laser Doppler anemometers (SLDA) in air-water layers simultaneously. The purpose of this study is to clarify turbulent structures in a wind-driven shear layer of each phase (air and water), and to evaluate the turbulent momentum transport phenomena across the air-water interface, and also to examine the transport from air-water interface to the water inertial flow.

INTRODUCTION

The scalar transfer phenomena across a gas-liquid interface have been observed in geophysical flows as well as in many industrial processes. Much attention has been focused on re-aerations of rivers and global-warming problems, especially as for environmentally issued gas such as CO_2, O_2 and NO_x. In addition to the above-mentioned matters, a closed system in water basins such as bays, lakes and "wando" (side-cavity in rivers) is considered necessary for the water environment because the ecosystem can be developed in such a heat and mass circulation area. Scientists and engineers engaged in these fields have developed some systems of the gas-liquid combined flows. It is, therefore, very important to investigate momentum, heat and mass transfer mechanism across the air/water interface. Recently, an accurate estimation of the scalar transport rate has been actively conducted on the basis of turbulence characteristics such as vortical cell theory and busting phenomena, e.g., see Komori *et al.* (4).

As for the transport phenomena across an air-water interface, it is essential to clarify the turbulent features in the free-surface region of water flows. Previous studies of wind-induced water-wave flows have been conduced in the coastal engineering and marine sciences. It is especially important to clarify the characteristic gas exchange mechanism across the air and water. Kawamura & Toba (2) have conducted some significant experiments on organized turbulent structures near the air-water interface of wind water waves, and they discussed the mutual interaction between the organized motions near the interface. Kawamura & Toba (8) indicated that there exists a turbulent boundary layer in the water flow, where hydrodynamic characteristics are dependent on the large-scale and low-frequency structure. They called its layer "the downward-bursting boundary layer (DBBL)". Yasuda *et al.* (9) investigated the wind-induced bursting layer near the air-water interface using a detailed spectrum analysis and pointed out that there existed a turbulent boundary layer near the wind-induced water surface, in which the enhanced Reynolds stress and the energy dissipation were closely related to the diffusion and the mixture of water body. Komori *et al.* (4) have proposed an eddy-cell model of air-water interfacial organized motions and discussed that an air-organized structure occurs intermittently near the windward interface of water wave crest and that it enhances the water coherent structure due to shear stress effects near the interface. However, few studies about instantaneous and coherent structures of the wind-driven water waves are available even now.

In previous studies, the conditional time-space correlation analysis and the u-v quadrant method have been intensively used to investigate coherent structures in shear flows. Nezu & Nakagawa (5) have developed a "half-threshold value quadrant method", and applied it to wall-turbulence phenomena in open channel flows. This method has been also applied to analyze the interfacial wind-induced shear flow by Nezu *et al.* (7). That is to say, the predominant structures and the Reynolds shear stress that seem to control the interfacial phenomena

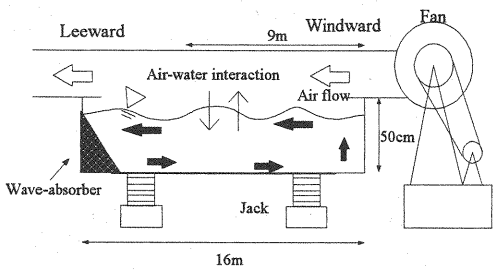

Fig.1 Air-water tunnel

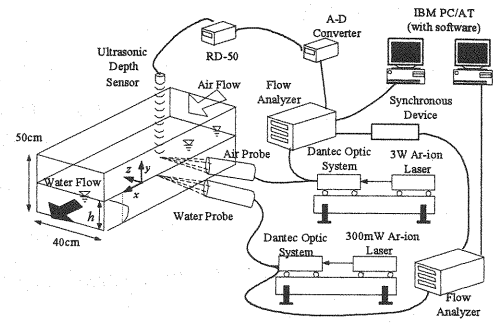

Fig.2 Arrangements of SLDA

Table 1 Hydraulic Conditions

Case	h (cm)	$U_{a,\max}$ (m/s)	U_{*a} (cm/s)	U_{*w} (cm)	U_s (cm/s)	η (cm)	H_s (cm)	L (cm)	f_p (Hz)
W1	20	4.24	18.5	0.450	0.54	0.035	1.17	8.16	4.9
W2		6.55	37.1	1.150	3.60	0.147	2.59	16.91	3.1
W3		9.06	54.0	1.730	4.98	0.763	3.48	22.42	2.6
W4		11.60	95.2	3.090	6.38	0.950	5.43	30.74	2.1

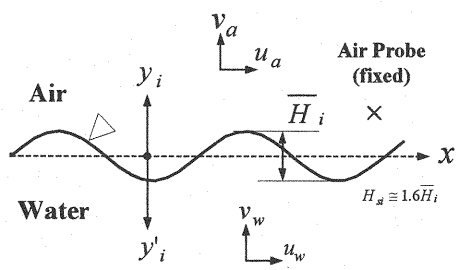

Fig.3 Coordinate system of SLDA

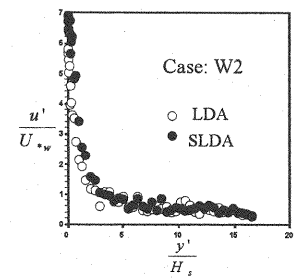

Fig.4 Comparison of LDA data with SLDA data

can be evaluated by using the *u-v* instantaneous velocity fluctuations. Kawamura & Toba (2) investigated the gravity wind waves, and evaluated the contribution of each quadrant event to the Reynolds stress. Komori *et al.* (4) estimated the frequency and the scale of the organized motions in wind-induced flow by using Variable-Interval Time-Averaging (VITA) method of Blackwelder & Kaplan (1).

Although some researchers have investigated turbulence and coherent structures in wind water waves, the interaction between air and water flows has not yet been evaluated clearly in these flows, in spite of their scientific and practical importance. The momentum transport mechanism between the surface water and the inertial water body has not been investigated so extensively. In the present study, turbulent structures were, therefore, measured along the vertical centerline of a closed wind-water channel by making use of two-sets of laser Doppler anemometers (SLDA).

EXPERIMENTAL PROCEDURES

Experiments were conducted in a 16m-long, 40cm-wide, 50cm-deep wind-water tunnel in which the channel slope was made to be adjusted. In this study, the channel slope was fixed to be horizontal, and the channel bed was hydrodynamically smooth. Figure 1 shows a schematic description of air-water tunnel in the present experiments. The sidewalls of the channel were constructed of the optical glass for LDA measurements from sidewall setting, as shown in Figure 2. The measurements were conducted at 9m downstream of the channel entrance, at which the flow field was fully developed, where the streamwise gradient of the turbulence

characteristics is almost neglected.

The coordinate system is shown in Figure 3. x and u are the streamwise axis and the velocity component, and y and v are the upward vertical axis from still water level and the corresponding velocity component. y' is the downward vertical axis from that. The subscripts a and w stand for air and water, respectively.

In the present experiments, two sets of synchronous laser Doppler anemometer systems (SLDA) were simultaneously used along the vertical direction in a closed water tank in order to measure the interaction between air and water flows. For all experimental cases, one LDA probe in the airside was set at each definite height y_i from the still water level, in which y_i was chosen here to be equal to $0.5\overline{H}_i$. $\overline{H}_i$ indicates the time-averaged wave height that was measured by several dozen of digital photos. The LDA measurements at y_i were not disturbed by the water waves. The other LDA probe in the waterside was moved vertically ($0.5\overline{H}_i \le y'_i < h$).

Table I shows the hydraulic conditions in this experiment. h is the fixed still water depth, $U_{a,\max}$ is the maximum air velocity which is evaluated by the mean velocity profile of the airflow. U_s is the approximated Eulerian water surface velocity. U_{*a} is the friction velocity in the airside, and U_{*w} is the friction velocity in the waterside, by evaluating the mean velocity profiles near the each interface from log-law. f_p is the predominant wave frequency which is analyzed by the power spectrum of streamwise velocity fluctuations. $\eta' \equiv \sqrt{\overline{\eta^2(t)}}$ is the intensity of air-water interface fluctuations $\eta(t)$. L is the time-averaged wavelength, and H_s is the representative wave height that was obtained by applying the Rayleigh-distribution law to experimental time-averaged wave height $\overline{H}_i$, that is, $H_s = 1.6\overline{H}_i$. The characteristics of the experimental conditions were measured at 9m downstream from the air inlet, as mentioned before. According to the classification of flow conditions in wind-induced water-waves flows by Kitaigorodskii (3) and Nezu *et al.* (6), the flow condition of Case W1 in the present experiments corresponds to the "smooth" interface, that of W2 to "ripple-waves" interface, and that of W3 and W4 to "two-dimensional gravity waves" interface. In the case of W4, the breaking waves with high frequency were often observed by human eyes behind the crests of gravity waves.

In this study, the SLDA was used in order to conduct simultaneous measurements of air and water velocities. Figure 4 shows an example of the comparison of streamwise turbulence intensity $u' \equiv \sqrt{\overline{u^2}}$ obtained from SLDA with that obtained from single LDA. The SLDA datasets are in a good agreement with LDA data, and therefore the SLDA technique is useful in evaluating the mutual turbulent relationship between air and water flows.

RESULTS AND DISCUSSIONS

Spectrum Analysis

Figures 5 (a) and (b) show the power spectra S_u and S_v of water velocity fluctuations u_w and v_w at the point of $y'/H_s \cong 1.0$ and 2.0, respectively, in the case of W2. Similarly, Figures 6 (a) and (b) show the distributions of S_u and S_v at $y'/H_s \cong 1.0$ and 2.0 in the case W4. The power spectrum is caluculated by Fast Fourier Transform (FFT). In these figures, the predominant frequency f_p is found in the band region from 1 to 10Hz, which indicates significant effects of wind-induced water waves on water velocity fluctuations. It was also observed that the spectrum distribution obeys the Kolmogoroff's –5/3 power law in the inertial subrange. The characteristics of power spectrum show that the wind-induced water-wave flows are so complicated that the water velocity fluctuations are composed of a few components, for example, a wind-drift current and an orbital motion, as pointed out by Yasuda *et al.* (9). Figures 7(a) and (b) show the power spectra of air velocity fluctuations at the point of $y/H_s \cong 0.5$ in the case of W2 and W4. The spectral profiles of streanwise velocity fluctuations S_{u_a} are different from those of the vertical fluctuations S_{v_a}. The value of S_{v_a} has a predominat component due to wave-induced effects. However, S_{u_a} has no dominant power region in the inertial spectrum subrange, that is similar to a wall shear flow such as open channel flows. Consequently, it is strongly suggested that the air flow over water waves is similar to a turbulent open channel flow except for vertical fluctuations due to the wave wave effects. In contrast, the water flow components u_w and v_w in wind water waves are greatly affected by wind water waves directly.

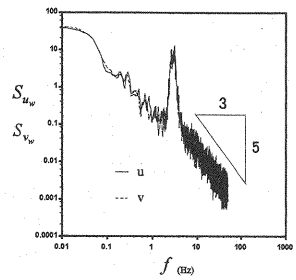

Fig.5(a) Power spectra S_{u_w} and S_{v_w} (Case: W2, $y'/H_S \cong 1.0$)

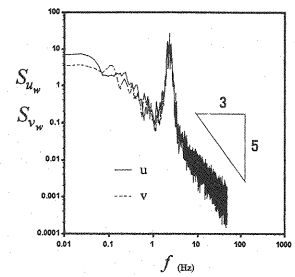

Fig.6(a) Power spectra S_{u_w} and S_{v_w} (Case: W4, $y'/H_S \cong 1.0$)

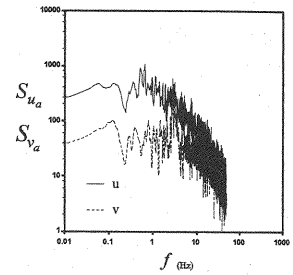

Fig.7(a) Power spectra S_{u_a} and S_{v_a} (Case: W2, $y/H_S \cong 0.5$)

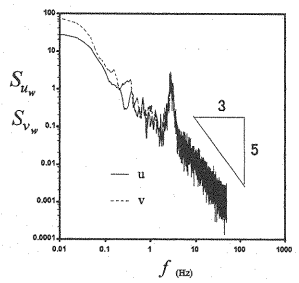

Fig.5(b) Power spectra S_{u_w} and S_{v_w} (Case: W2, $y'/H_S \cong 2.0$)

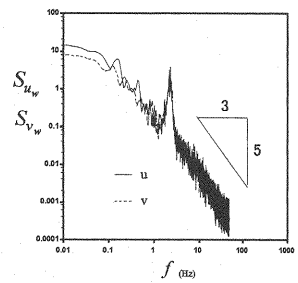

Fig.6(b) Power spectra S_{u_w} and S_{v_w} (Case: W4, $y'/H_S \cong 2.0$)

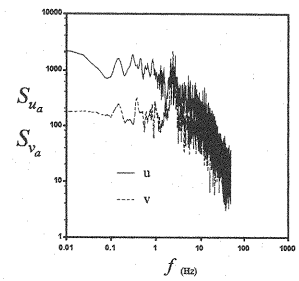

Fig.7(b) Power spectra S_{u_a} and S_{v_a} (Case: W4, $y/H_S \cong 0.5$)

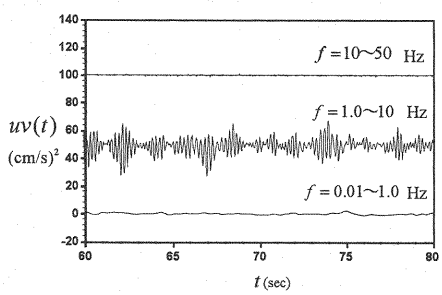

Fig.8 (a) Time series of instantaneous Reynolds stress $uv(t)$ (Case: W4, $y'/H_s \cong 1.0$)

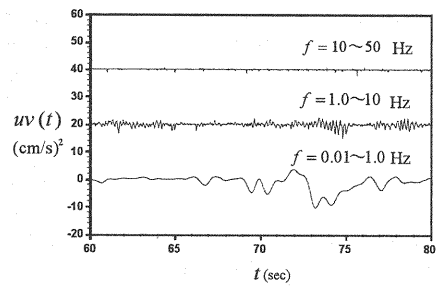

Fig.8(b) Time series of $uv(t)$ (Case: W4, $y'/H_s \cong 2.0$)

Filter Analysis

The linear filter-conducted water velocity fluctuations are given by

$$u_{wk}(t) = \sum_{k=k_a}^{k_b} \sqrt{2S(f_k)\Delta f_k}\,\cos(2\pi \overline{f_k} t + \theta_k) \quad \text{for} \quad k_a < k < k_b$$

, in which $\overline{f_k} = (f_k + f_{k-1})/2$ and $\Delta f_k = f_k - f_{k-1}$ (1).

f_k is the k-th ($k \in N$, a natural number) frequency in the Fourier space and θ_k is the phase delay in the Fourier transform. In general, the linear filter is not a complete re-constructive filter so that each filter-conducted velocity fluctuations do not exactly re-compose the original velocity fluctuations. It may be considered that a linear filter could be an approximated filter estimation method of velocity fluctuations.

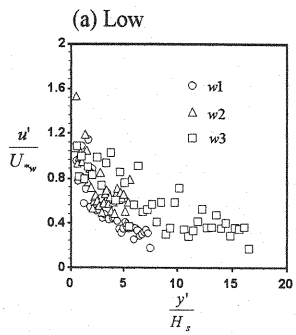

Fig.9 (a) Turbulence intensity u' (Low frequency-filtered)

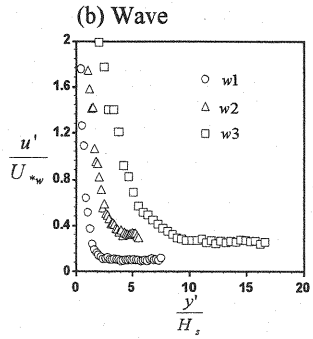

Fig.9 (b) Turbulence intensity u' (Wavy frequency-filtered)

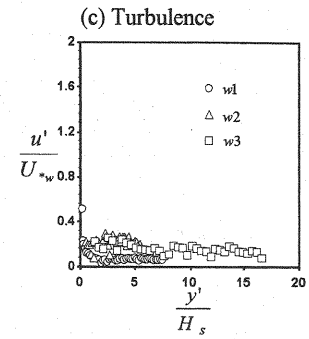

Fig.9 (c) Turbulence intensity u' (High frequency-filtered)

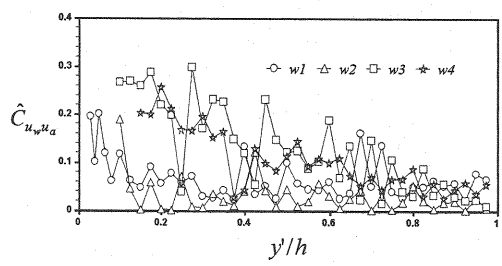

Fig.10 Distribution of $\hat{C}_{u_w u_a}(\tau, y')$ versus y'

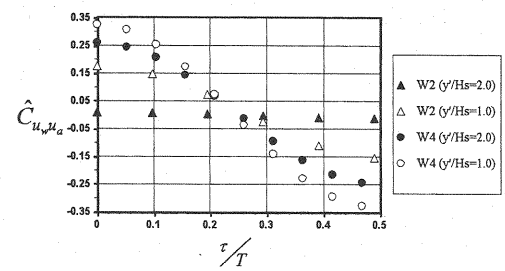

Fig.11 Distribution of $\hat{C}_{u_w u_a}(\tau, y')$ versus τ

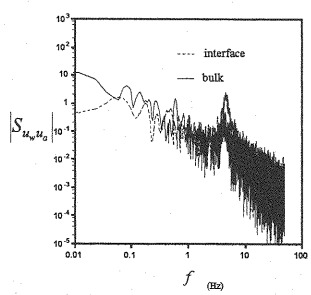

Fig.12(a) Absolute value of cross spectrum $|S_{u_w u_a}|$ (Case: W2)

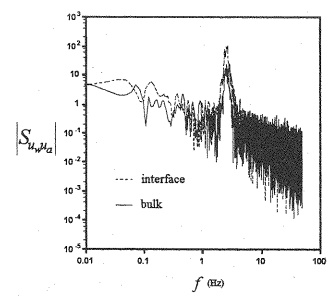

Fig.12(b) $|S_{u_w u_a}|$ (Case: W4)

In this study, three kinds of frequency filters were used to evaluate the original water velocity fluctuations; 1) **Low**; low pass filter (0.01～1Hz), 2) **Wavy**; wave-frequency band pass filter (1～10Hz) and 3) **Turbulence**; high pass filter (10～50Hz). Figures 8(a) and (b) show some examples of linear filter-conducted instantaneous Reynolds stress $uv(t)$ at the point of $y'/H_s \cong 1.0$ and 2.0 in the case of W4. It was observed that there was the difference of momentum transport between the wave-filtered and low-filtered fluctuations at two different vertical points. Figures 9(a), (b) and (c) show the distributions of tubulence intensity that were normalized by the waterside friction velocity U_{*w}. In these figures, it should be noted that the low and turbulence components are in a good agreement with each other among three cases. This means that the interfacial water flow may obey a similarlity law in the shear flow caused by wind-drift currents.

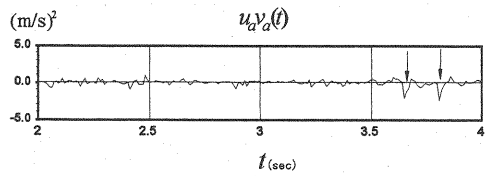

Fig.13 Time series of air flow (Case: W4)

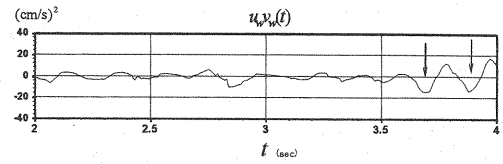

Fig.14 Time series of water flow (Case: W4)

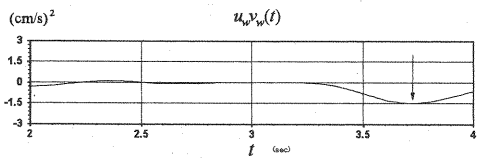

Fig.15(a) Time series of water flow (Case: W4) (Low-frequency filter)

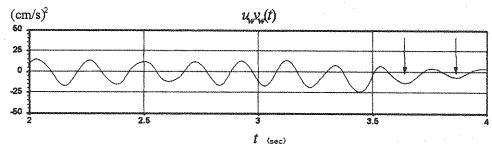

Fig.15(b) Time series of water flow (Case: W4) (Wavy-frequency filter)

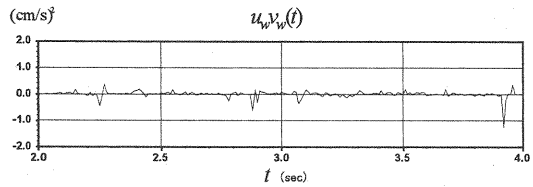

Fig.15(c) Time series of water flow (Case: W4) (High-frequency filter)

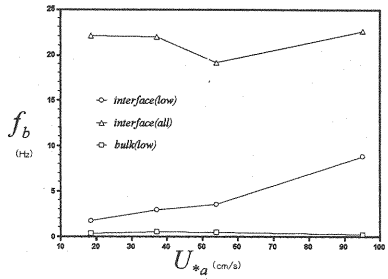

Fig.16 Frequency of bursting phenomena f_b

Air-Water Interaction

Since air-water simultaneous velocity measurements were conducted, the normalized cross-correlation coefficient $\hat{C}_{u_w u_a}(\tau, y')$ is defined as follows:

$$\hat{C}_{u_w u_a}(\tau, y') = \frac{\overline{u_w(y', t) u_a(y_a, t+\tau)}}{u_w'(y') u_a'(y_a)} \tag{2}$$

where τ is the time lag. Figure 10 shows the maximum values of $\hat{C}_{u_w u_a}(\tau_{\max}, y')$ against the distance y'. Figure 11 shows the value of $\hat{C}_{u_w u_a}(\tau, y')$ against the time τ for $\tau < 0.5T_p$, in which $T_p = 1/f_p$. The values of $\hat{C}_{u_w u_a}$ are relatively large in the free-surface region, and there is no difference in these values below the half water depth. It was also found that the value of $\hat{C}_{u_w u_a}$ becomes larger as the wind becomes stronger. Its correlation value doubled in magnitude when the water wave patterns changed. The reason for this is that the flow condition changes from three-dimensional (3-D) ripple flow to 2-D gravity-wave one. On the other hand, the water flow mechanism is very sensitive to air-water interface, especially to the wave motions, as compared with the air flow. Figures 12(a) and (b) show the absolute values of the cross spectrum in the interface region and the bulk region (half-depth region) in the case of W2 and W4. The cross spectrum $S_{u_w u_a}$ is calculated from the Wiener-Khintchine equation using the value of $\hat{C}_{u_w u_a}$. Figure 12 shows clearly that when the wind blows stronger, the wavy component has a great influence on the cross correlation between air and water flows. It was also observed that the value of cross–correlation at the bulk elevation is similar to that of the interfacial elevation except for the wavy components (1～10Hz). This may explain why the wind wave patterns affect only wavy component of cross-correlation between air and water velocity perturbations and have an significant influence on

quantitative interactions between air and water flows.

Figures 13 and 14 indicate the time series of instantaneous Reynolds stress of air flow and water flow in the case of W4. Two data were measured simultaneously. In these figures, the bursting-like event occurred on both the air and water flows (the downward-pointing arrows show the bursting event). When the large Reynolds stress appeared in air flow (an ejection type; $u_a<0, v_a>0$, $u_a v_a<0$), the relatively large Reynolds stress was observed in water flow (a sweep type; $u_w>0, v_w<0$, $u_w v_w<0$). Figures 15(a), (b) and (c) show the filter-conducted waterside Reynolds stresses, which were obtained from the original data of Figure 14. When the bursting phenomena occur in flows, a relatively large low-frequency water perturbation is observed in water flow, as shown in Figure 15(a). This is why the low frequent fluctuations in water flow are key factors in bursting phenomena of wind-induced water waves. It is also pointed out that the wave-frequency motions are effective in momentum transport from the interface to the inertial water body. However, this wavy motion does not control the busting phenomena because the Reynolds stress caused by wavy-frequency component is relatively small at the time of bursting event than at the other times (see Fig.15(b)).

Figure 16 shows the frequency of busting phenomena for two kinds of data, that is, the original water fluctuations (**all**) and low-frequency fluctuations (**low**) at the different vertical points (**interface**; $y'/H_s \cong 1.0$ and **bulk**; about half water depth), that were evaluated by the 'half-value threshold quadrant method' of Nezu & Nakagawa (5). It was observed that the low-frequency bursting frequency increases with an increase of the air friction velocity U_{*a} on the interface. The bursting phenomenon was not observed clearly in the original water fluctuations, because the data are composed of complex combined fluctuated flows, as mentioned previously. Therefore, it is very probable that the low-frequent fluctuations are the main governing components of bursting phenomena in wind-induced water waves flows.

CONCLUDING REMARKS

In this study, a number of synchronous LDA (SLDA) measurements were conducted in order to analyze space-time correlations between air and water velocities and also to evaluate the interaction between the two flow phases in wind-induced water-wave flows. Findings reveal that the low-frequent water velocity fluctuations contribute to the bursting phenomena in water flows. This flow mechanism changes dynamically as the wind blows stronger; that is to say, the interaction between two flow phases is larger as the water-wave pattern changes from 3-D ripples to 2-D gravity waves. The following results are summarized in this study:

1) The airflows over the wind-induced water-waves are similar to the flow over the bottom bed in open-channel flows, except for the relatively large vertical fluctuations near the fixed interface.
2) There exists a significant interaction between the air and water flow in wind-induced water waves flows. The low-frequent bursting-like events on the airside near the free surface induce the downward bursting phenomena near the movable interface on the waterside.

ACKNOLEDGEMENTS

The present study was made possible thanks to the financial support from the Research Project Grant-In-Aid for Scientific Research No. (B)(2) 12450200 (Representative: I. Nezu) of Japanese Government. The authors gratefully acknowledge this support.

REFERNCES

1. Blackwelder, R.F. and Kaplan, R.E.: On the wall structure of the turbulent boundary layer, *J. Fluid Mech.*, Vol.76, pp.89-112. 1976.
2. Kawamura, H. and Toba, Y.: Ordered motion in the turbulent boundary layer over wind waves, *J. Fluid Mech.*, Vol.197, pp.105-138, 1988.
3. Kitaigorodskii, S.A. and Donelan, M.A. : Wind-wave effects on gas transfer, *Gas Transfer at Air-Water Interfaces*, (eds. W. Brutsaert and G.H. Jirka), pp.147-170, 1984.
4. Komori, S., Nagaosa, R. and Murakami, Y.: Turbulence structure and mass transfer across a sheared air-water interface in wind-driven turbulence, *J. Fluid Mech.*, Vol.249, pp.161-183, 1993.
5. Nezu, I. and Nakagawa, H.: *Turbulence in Open-Channel Flows*, IAHR-Monograph, Balkema, 1993.
6. Nezu, I., Nakayama, T. and Inoue, R.: Turbulence structure in air-water interface with wind shear, Annual Journal of Hydraulic Engineering, Vol.43, pp413-418, 1999 (in Japanese) .
7. Nezu, I., Ushijima, S. , Onitsuka, K. and Yoshida, K.: PIV measurements of turbulent structures across air-water interface in wind-driven water waves, 6th Asian Symp. on Visualization, Pusan, Korea, pp.363-365

(full paper on CD-ROM), 2001.
8. Toba, Y. and Kawamura, H.: Wind-wave coupled downward-busting boundary layer (DBBL) beneath the sea surface, *J. Oceanography*, Vol.52, pp.409-419, 1996.
9. Yasuda,T., Mizutani, N, Itano, S, Isaka, K., Kawagoe, Y. and Onoda, T.: Water surface bursting layer generated by strong winds and its turbulence characteristics, *Proc. of Coastal Engineering, JSCE*, Vol.47, pp106-110, 2000 (in Japanese) .

APPENDIX - NOTATIONS

The following symbols are used in this paper:

$C_{u_w u_a}$ = cross correlation coefficient between u_w and u_a;
f = frequency ;
f_p = predominant frequency of water waves;
h = water depth of wind-tunnel tank;
H_s = wave height of representative waves;
$\overline{H}$ = time-averaged wave height;
L = wave length of water waves;
S = power spectrum;
$S_{u_w u_a}$ = cross spectrum between u_w and u_a;
T_p = predominant period, $T_p \equiv 1/f_p$;
u = streamwise component of velocity fluctuations;
u' = streamwise turbulence intensity $\left(\equiv \sqrt{\overline{u^2}}\right)$;
$U_{a,\max}$ = maximum air velocity;
U_{*a} = air-side friction velocity on the air/water interface;
U_{*w} = water-side friction velocity on the air/water interface;
v = vertical component of velocity fluctuations;
v' = vertical turbulence intensity $\left(\equiv \sqrt{\overline{v^2}}\right)$;
x = streamwise coordinate;
y = upward vertical coordinate from the air/water still interface;
y' = downward vertical coordinate from the air/water still interface, i.e., $y' \equiv -y$;
η = amplitude of fluctuations of free surface from the still water level;
η' = surface fluctuation intensity $\left(\equiv \sqrt{\overline{\eta^2}}\right)$
τ = lag time;
suffix a = air value; and
suffix w = water value.

(Received July 1, 2002 ; revised January 10, 2003)